THE JOURNAL OF PHYSICAL CHEMISTRY B

Article

pubs.acs.org/JPCB

High Strength of Physical Hydrogels Based on Poly(acrylic acid)-*g*-poly(ethylene glycol) Methyl Ether: Role of Chain Architecture on Hydrogel Properties

Jun Yang,[†,‡] Cheng Gong,[†] Fu-Kuan Shi,[†] and Xu-Ming Xie*[,†]

[†]Advanced Materials Laboratory, Department of Chemical Engineering, Tsinghua University, Beijing, 100084, China

[‡]College of Materials Science and Technology, Beijing Forestry University, Beijing, China

ABSTRACT: This investigation was to study the connections between polymer branch architecture of physical hydrogels and their properties. The bottle-brush-like polymer chains of poly(acrylic acid)-*g*-poly(ethylene glycol) methyl ether (PAA-*g*-mPEG) with PAA as backbones and mPEG as branch architecture were synthesized and in situ grafted from silica nanoparticles (SNs) to construct hydrogels cross-linked networks in aqueous solutions. The structural variables to be discussed included molecular weight and molar ratio of branch chains, and new aspects of the formation mechanism of physical hydrogels with branch structure in the absence of organic cross-links were present. The results indicated that the differences of polymer chain architecture could be distinguished via their different interactions that are present by gelation process and mature gel properties, such as gel strength and swelling ratio. The gelation occurred at the critical polymer concentration and molecular weight, respectively, and the inorganic/organic (SNs/PAA-*g*-mPEG) nanoparticles began to entangle and construct the cross-linking networks afterward. The gel-to-sol transition temperature ($T_{g\text{-}s}$) and radii of SNs that were encapsulated by polymer chains as a function of time for chains' disentanglement were monitored according to the observation of the dissolution process, and the molecular weight between two consecutive entanglements (M_e) was calculated thereafter. This study showed that the introduction of branch chain onto the linear backbone significantly promoted the chain interactions and increased entanglement density, which contributed to the hydrogels' network integrity and rigidity, thus illustrating greater elongation at break and tensile strength than the hydrogels formulated with linear polymer chains.

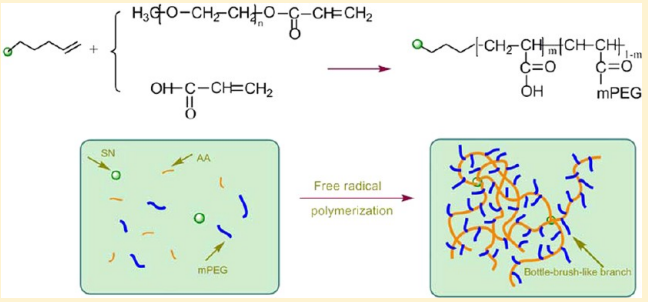

1. INTRODUCTION

Hydrogels are cross-linked three-dimensional networks of water-soluble polymeric materials that swell to several times their own weight in the presence of water or biological fluids, yet cannot fully dissociate due to the presence of network cross-links.[1−3] Consideration their high water content, rubberlike state, and biocompatibility, hydrogels are very useful in many fields, such as drug delivery systems, biomedical devices, and tissue engineering.[4,5] However, the fragility of most hydrogels poses a formidable obstacle to their applications where high mechanical strength is required, and there is growing considerable progress in efforts to solve this problem.[6,7] Gong et al. worked on double network hydrogels that greatly enhanced the fracture toughness by increasing the dissipative volume ahead of the crack point.[8] Okumura et al. prepared a sliding double ring cross-link by cross-linking two cyclodextrin molecules on poly(ethylene glycol) (PEG) chains and the hydrogels possessed both excellent swelling ratio and mechanical properties.[9] Haraguchi et al. contributed to some progress on organic−inorganic hybrid nanocomposites by introducing inorganic clay as unique cross-linking points to synthesize hydrogels with extraordinary extensibility, high strength, and transparency.[10,11] Huang et al. reported irradiating the macromolecular microsphere composite and the hydrogels exhibited extremely high mechanical strength under compression.[12]

It has been recognized for decades that chain entanglement is central to determine the ultimate properties of flexible polymers, affecting both flow behavior of molten and mechanical properties in the solid state.[13−15] The models of entanglement assume that localized entanglements or temporary cross-links could be visualized as knots or local interactions, which restrict the chain's mobility.[16,17] The theoretical development of these models is based on the statistical treatment of network with non-Gaussian chains, and the architecture of the polymer is assumed to be constituted of long molecular chains randomly distributed in space. The physical links are, in general, not permanent and may change depending on strain and the effect of branching architecture on the polymer molecular properties is a fundamental topic.[18−20] The branch length and branch density can be tailored by the molecular weight of macromonomer and reaction conditions,

Received: April 18, 2012
Revised: August 27, 2012
Published: September 5, 2012

dx.doi.org/10.1021/jp303710d | *J. Phys. Chem. B* 2012, 116, 12038−12047

and many reports have shown that poly(macromonomer)s with branching architecture exhibit many important properties, such as very high melt viscosities, toughness, and elastomeric viscoelasticity.[21−23]

There is much literature about the preparation of physical gels; however, for dilute solution of polymer chains in the presence of inorganic component (silica particles) as multifunctional cross-links, much less has been reported.[24,25] In our earlier work,[26,27] a simple platform capable of synthesizing tough and flexible nanocomposite hydrogels was proposed. The silica nanoparticles (SNs) and acrylic acid (AA) were applied as starting materials, and the free-radical polymerization occurred in an aqueous solution with propagating poly(acrylic acid) (PAA) macroradical on the surface of SN. The linear PAA chains grafted from the surface of SN to produce entanglements (physical junctions), and thus these flexible chains collected the neighboring silica particles together and built a network structure. At the initial stage of the gelation process, the system presented a solution state, and then gel point occurred as the polymer chains grew to a critical length where the interaction of entanglement was strong enough to maintain network rigidity. The soluble fraction comprised linear structures of finite molecular weight which would be intimately entangled like the permanent chemical networks, and the water-insoluble hydrogel obtained beyond the gel point. Consequently, these trapped and nonpermanent physical entanglements contributed to the networks' formation, and the SNs restricted the number of available chain configurations, and thus served similar effects to the chemically cross-links (Figure 1). Although some efforts have been made to explore

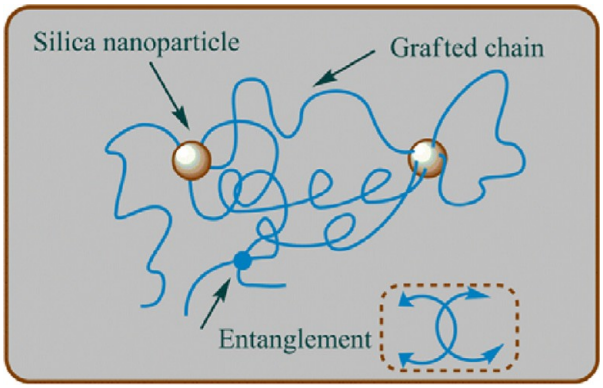

Figure 1. Schematic representation of the inorganic/organic network structure. Many flexible polymer chains graft on the SNs surface and collect them together, where two chains that cannot pass through one another form topological interactions (entanglement) that act as temporary cross-links.

the effects of molecular weight of the grafted chain, water content of network, and diameter of SNs on hydrogels' properties, which are naturally important parameters for the hydrogels properties, the comprehensive characterization of the influence of polymer chains architecture on network structure is still unknown.[26,27] Thus, with an aim of understanding the effects of branch structure on gelation process, the goal of this study is to pursue the influence of strengthening entanglements effect by incorporation of branch chain on linear backbone chains, including gelation rate, swelling ratio, and mechanical properties. To accomplish this, we prepared a series of hydrogels based on poly(acrylic acid)-*g*-poly(ethylene glycol) methyl ether (PAA-*g*-mPEG) with various degrees of entanglements by tailoring bottle-brush-like branch chains on backbone chains with PAA as linear backbone and mPEG as branch architecture. Furthermore, in order to monitor the polymer chain structural changes around the gel point, we are interested in monitoring the critical molecular weight, M_{crit}, for the gelation onset and chains' entanglement. The results indicate that the branch architectures prominently affect the intermolecular chain entanglement couplings, swelling behavior, and mechanical properties, and thus contribute to the networks formation and integrity.

2. MATERIALS AND METHOD

2.1. Materials. Poly(ethylene glycol) methyl ether (mPEG, M_w = 750, 2000, and 5000 Da) was purchased from Sigma-Aldrich. Acryloyl chloride was purchased from Beijing HengYeZhongYuan Chemical Co., China. Acrylic acid (AA), triethylamine (TEA), ammonium persulfate, γ-methacryloxypropyltrimethoxysilane (A-174), tetraethyl orthosilicate (TEOS), ammonium hydroxide (28 wt %), ammonium persulfate (APS), and other reagents were all analytical grade and used without further purification. Deionized water was used for all experiments and oxygen present in the water was removed by bubbling nitrogen gas for 30 min prior to use.

2.2. Preparation and Modification of Silica Nanoparticles. The silica nanoparticles (SNs) were prepared via the well-known Stöber procedure by hydration of TEOS in diluted alkaline solution.[28] A mixture of ethanol (43 mL) and aqueous ammonia (28 wt %, 2 mL) was mixed and stirred at room temperature for 2 h, then the predetermined tetraethyl orthosilicate (6.1 mL) was slowly added to the solution. After 24 h the crude silica suspension was purified by ultrafiltration with water and a stable suspension of SN was obtained (5 wt %), with an average radius r and a specific surface area δ of 210 nm and 6.55 m^2/g, respectively. The obtained SNs were surface modified by silane coupling agent (A-174), thereby the exposing vinyl groups were applied to react with the AA monomer during polymerization.

2.3. Preparation of mPEG Monoacrylate. The synthetic procedure of mPEG monoacrylate was similar for all the samples with three kinds of molecular weight (Figure 2). In a

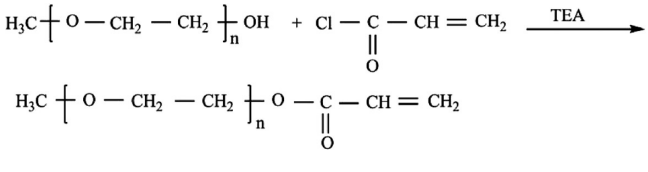

Figure 2. Synthesis of mPEG acrylate.

typical experiment, toluene (80 mL), mPEG 750 (7.5 g), and triethylamine (10 mL) were added into a three-neck flask, then acryloyl chloride (2.25 mL) was slowly added into the flask. The mixture was stirred under N_2 atmosphere for 12 h at 30 °C. Subsequently, mPEG acrylate was purified by a precipitation-extraction procedure with hexane solvent to remove unreacted macromonomer, and then dried under vacuum at 35 °C for 24 h. The specific conditions are shown in Table 1.

2.4. Preparation of Hydrogel with Branch Architecture. The hydrogels' synthetic procedure described herein is similar to that reported previously.[26,27] For example, to prepare PAA-*g*-mPEG 2000 hydrogel, a solution of water (30 mL, for all

dx.doi.org/10.1021/jp303710d | J. Phys. Chem. B 2012, 116, 12038−12047

Table 1. Reaction Conditions for Synthesis of mPEG Monoacrylates

sample	mPEG (g)	toluene (mL)	triethylamine (mL)	temp (°C)	time (h)	yield (%)
mPEG acrylate (750)[a]	7.5	80	10	30	12	94.5
mPEG acrylate (2000)	20	130	15.5	45	30	93.2
mPEG acrylate (5000)	50	185	21.3	52	35	91.4

[a]Numbers in parentheses denote the molecular weight of mPEG used for acrylate reaction.

cases), inorganic silica (0.07 g), AA (5 mL, for all cases), and mPEG acrylate (1.4 g) was prepared. Then, the solution was allowed ultrasonic dispersion (100 W) in an ice-water bath for 20 min to produce a homogeneous suspension, and dissolved gases were removed under vacuum for 10 min. Next, an aqueous solution of initiator (APS, 0.14 g in 3.5 mL of H_2O) was added into the above degassed solution while stirring and the free-radical polymerization was allowed to proceed in an oil bath at 65 °C for 2−4 h under N_2 atmosphere (Figure 3). For mechanical property tests, hydrogels were used as-prepared to keep the water/polymer weight ratio equal to that of initial gel samples, unless otherwise mentioned. The dry hydrogels were prepared by drying as-prepared hydrogels at 65 °C in an oven with air circulation for 48 h and then at 60 °C in a vacuum oven for another 24 h. The hydrogel compositions and the molecular characteristics of these polymer chains are shown in Table 2.

2.5. Screen of Gel Formation. Rapid screening of gel formation time was performed by visual inspection as follows: for a reaction solution in the beaker with a stirring bar (6 × 3 mm, 150 rpm), a stopwatch was started. The approximate gel formation time was recorded when the stirring bar stopped rotating as a result of gel formation and the specific gelation process characterization was performed by dynamic rheology measurement. In addition, in order to carefully study the influence of branch length on gel point, the beakers with the above reactants were removed from the bath at different time intervals. The solution was transferred into an ice-water bath at different time intervals and the reaction was quenched. The monomer conversion ratio was measured by subsequent dialysis against water for 4 days (molecular weight cutoff 7500 Da), dried in the vacuum oven at 80 °C for 48 h, and weighed.

2.6. Characterization. *IR and NMR.* The FT-IR spectra were recorded by a Thermo Scientific, Nicolet 6700, through the KBr pellet method. ^1H NMR spectra measurements were performed on a JNM-ECA600, JEOL (Japan) NMR spectrometer operating at 600 MHz, using deuterated chloroform ($CDCl_3$-*d*) as solvent and tetramethylsilane (TMS) as an internal standard.

Swelling Ratio. The swelling ratio experiment was performed by immersing dried hydrogel (6 mm in diameter and 3 mm in height) into excessive water at 25 °C (2 L, the water was changed each time the gel weight was measured), and the sample was taken out at certain time intervals, blotted with a filter paper to remove water on the surface, and weighed. The swelling ratio was calculated by the ratio of swollen hydrogel weight (W_{wet}) to the corresponding dried hydrogel (W_{dry}). Three swelling ratio experiments were conducted for each sample to ensure reproducibility.

Gel-to-Sol Measurement. The hydrogels (~1 g) were immersed into water (~10 L) under different temperatures (in range of 45−78 °C) and the transition was monitored by measurement of mass loss as a function of time until bulk dissolution. The swollen hydrogels were taken out at certain time intervals and dried (vacuum oven at 80 °C) for mass loss calculation. To examine the changes of the hydrodynamic radii (r) of SNs within the gel-to-sol transition, a certain amount of the above aqueous solution was applied to detect via dynamic light scattering (DLS, Zetasizer 3000HS, Malvern Instruments) measurements under temperature-regulated cell with a He−Ne laser (wavelength of 633 nm and power of 10 mW). Scattered light was collected at an angle of 90° by a photon-counting photomultiplier tube and the result was expressed as the *Z*-average mean which was the harmonic intensity averaged particle diameter. The measurements were performed at 65 °C (unless otherwise stated), in triplicate, with 5 min runs, using a 400 μm aperture. The samples for DLS experiment were prepared in a test cuvette (square glass in 12 mm) after

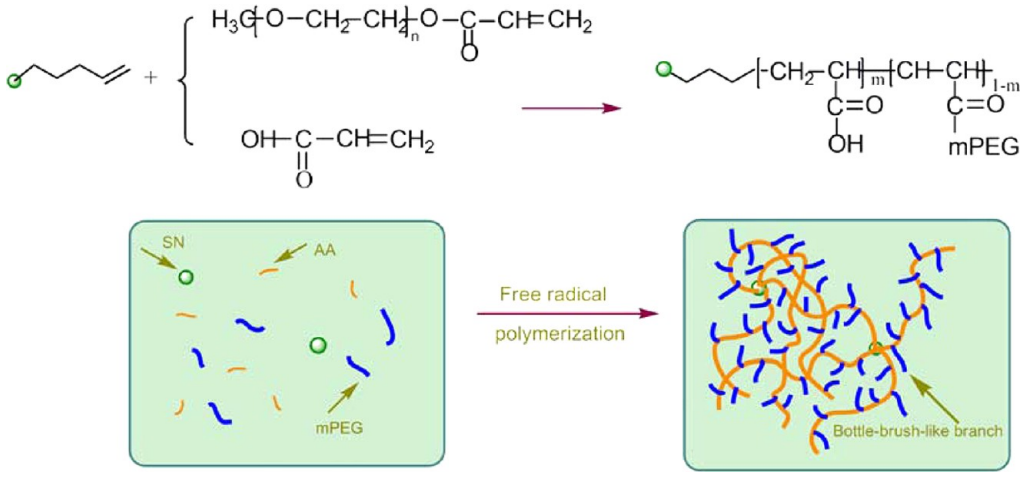

Figure 3. Schematic illustration of the backbone chain (PAA) with bottle-brush-like branch structure (mPEG acrylate) in situ graft from the surface of silica nanoparticles (SNs). The entanglements among grafted polymer chains contribute the uniformly dispersed SNs serving as physical cross-links to form the network structure (only a small number of polymer chains are depicted for simplicity).

dx.doi.org/10.1021/jp303710d | J. Phys. Chem. B 2012, 116, 12038−12047

Table 2. Raw Compositions and Characteristics of Poly(macromolecule)s for Hydrogel Preparation

			total		backbone		branch	
sample	SNs (mg)	APS (mg)	M_w (10^{-4})	PDI	M_w (10^{-4})	PDI	M_w	mol % of backbone chain[a]
PAA	70	5	7.16	1.88	–	–	–	–
PAA-*g*-mPEG 750-a	70	18	7.65	2.13	7.23	1.63	750	1
PAA-*g*-mPEG 750-b	70	21	7.92	2.25	7.24	1.73	750	2.5
PAA-*g*-mPEG 750-c	70	92	8.13	2.32	7.27	1.67	750	5
PAA-*g*-mPEG 2000	70	140	6.94	2.37	7.33	1.69	2000	1
PAA-*g*-mPEG 5000	70	154	7.88	2.45	7.31	1.71	5000	1

[a]Molar percentage of mPEG to AA.

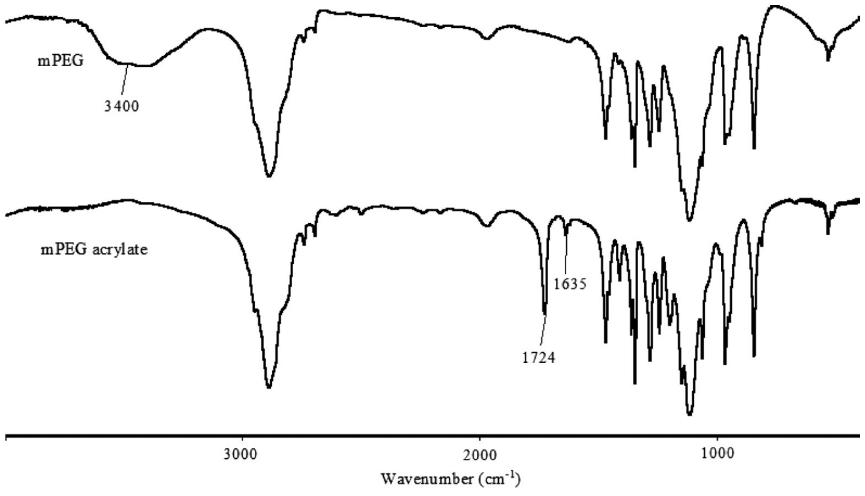

(a)

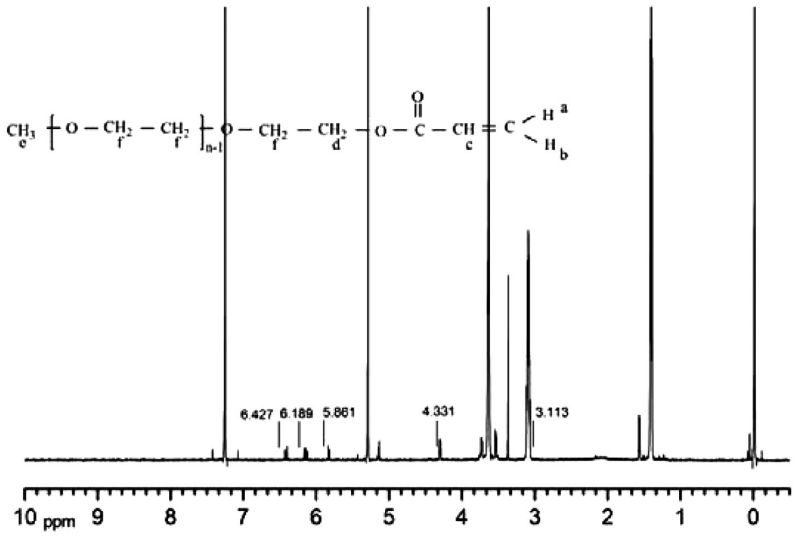

(b)

Figure 4. FTIR (a) and ^{1}H NMR (b) spectra of mPEG acrylate.

filtration of any possible trace of gelation solutions through nylon membrane filters with a pore size of 1 μm.

Transmission Electron Microscopy. The synthesized hybrid gels were imaged on a JEM-1010 (JEOL) transmission electron microscope (TEM) at an acceleration voltage of 60 kV. The dilute suspension of the sample was first sonicated (100 W) for 10 min in an ice-water bath, then several drops of sonicated suspension were deposited onto a standard holey carbon-

dx.doi.org/10.1021/jp303710d | J. Phys. Chem. B 2012, 116, 12038−12047

coated copper grid, and the grid was then dried overnight by a vacuum oven at 25 °C.

Mechanical Properties. For mechanical properties measurement, the hydrogels were tested using an electronic universal material testing machine (Gotech Testing Machines Inc., GT-TS-2000) under following conditions: cross-head speed = 30 mm/min, gauge length = 20 mm, and hydrogel size = 10 mm in width × 15 mm in length × 30 mm in height. The initial cross section (150 mm^2) was used to calculate the tensile strength at breaking point. For any of the conditions tested, 2−3 samples were used to confirm the reproducibility and no significant differences were used to confirm the reproducibility.

Molecular Weight. The dried SN gel (~0.5 g) was cut into small pieces and immersed into hydrofluoric acid solution (50 mL, 20 wt %) for 24 h under stirring (25 °C) and was neutralized by the addition of sodium carbonate solution (0.5 moL/L); then the solution was filtered (pore size of the poly(tetrafluoroethylene) membrane discs was 0.45 μm). The molecular weight of graft chain was measured by size exclusion chromatography (SEC) (Tosoh Bioscience, TSK-GEL $G3000SW_{XL}$ 300 mm × 7.8 mm). The solution was diluted to 5 mg/mL in phosphate buffer (0.01 mol/L NaH_2PO_4 and 0.02 mol/L Na_2HPO_4, pH 7) and the degassed phosphate buffer was used as mobile phase at flow of 0.25 mL/min. The monodisperse dextran standard samples that obtained from Pharmacia Biotech Corp. were used to obtain a universal calibration curve for calculating the molecular weight and polydispersity index (PDI) of the polymers herein.

Viscosity Measurements. The oscillatory shear rheology measurement was conducted by a Physica MCR301 (Antor Paar Rheometer), operating with cone geometry (CC27, 26.667 mm in diameter, 40.026 mm in length) under N_2 atmosphere at 70 °C. To minimize dehydration, a thin layer of low-viscosity silicone oil was employed on the sample surface. The values of storage modulus (G') and loss modulus (G'') were recorded between the frequency ranged from 0.01 to 100 Hz at a strain of 1%, which was within the linear viscoelastic region as determined by dynamic strain sweep experiments.

3. RESULT AND DISCUSSION

3.1. Characterization of mPEG Acrylate. According to the FT-IR analysis (Figure 4a), it was obvious that mPEG showed a broad peak at 3400 cm^{-1} correspondence to stretching vibration of −OH, and it disappeared on the spectrum of mPEG acrylate. The strong and acute peaks at 1724 and 1635 cm^{-1} corresponding to the stretching vibrations of −O−C═O and −C═C−, respectively, were also observed in the spectrum of mPEG acrylate. In addition, the Figure 4b shows the ^1H NMR spectrum of mPEG acrylate: 3.5−4 ppm resonance peaks assigned to the protons of $(-CH_2-CH_2-O-)_n$ (f), intense resonance peaks appearing at 6.4, 6.1, and 5.8 ppm that were assigned to the protons of $CH_2{=}CH-$ (a, b, c). The peak at 4.3 ppm corresponded to the protons of $-CH_2-COO-CH{=}CH_2$ (d), while the peak at 3.1 ppm assigned to CH_3-O- (e). The above FTIR and ^1H NMR spectra confirmed that the mPEG acrylate was successfully synthesized.

3.2. Branch Architecture on Gelation. The water-soluble mPEG acrylate was able to be homogeneously mixed with the aqueous solution of AA and SNs, and the monomers (AA, mPEG acrylate) grafted from the SNs surface via radical polymerization that was initiated by ammonium persulfate. The obtained hydrogels were yellow, rubberlike with excellent flexibility (Figure 5). The dispersion of SNs was examined by

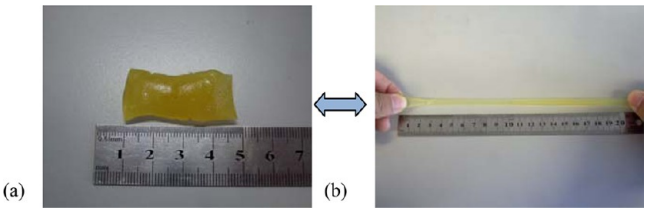

Figure 5. Photos of as-prepared hydrogel PAA-*g*-mPEG 750-a gel (a) and after its elongation (b).

TEM observation (Figure 6) and it indicated that the SNs encapsulated by grafted polymer chains dispersed uniformly in

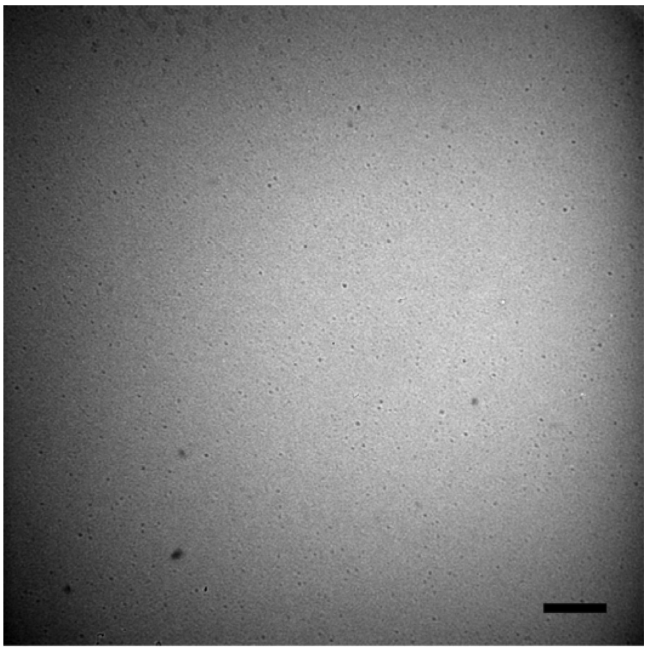

Figure 6. Transmission electron micrograph of dried PAA-*g*-mPEG 750-a gel. (bar = 5 μm).

the polymer matrix. In fact, even in the dried state, the SNs dispersed well throughout the polymer matrix. Since the SNs in the dry gel were in a concentrated state (0.2 wt % against polymer), which still exhibited good dispersion, it can be concluded that the homogeneous dispersion of PAA/SN network structure with the swelling hydrogel was achieved. Besides, the diameter of SN was mainly observed at ~430 nm, which was consistent in the size of SNs applied in hydrogel preparation.

To examine the gel formation process, the rheological behavior of gelation with time in the case of PAA-*g*-mPEG 750-a was measured and the values of G' and G'' as a function of frequency at three typical time points were shown in Figure 7. At the initial stage of polymerization (20 min), $G' < G''$, the viscous properties dominated the liquid state. As the reaction proceeded, the system gained elastic properties resulting in a gel-like state of the hydrogel composite. Although both of the moduli increased, the slope of G' with respect to time was higher than that of G''. This difference in the rate led to a point of crossover of G' and G'' ($G' \sim G'' \sim \omega^n$), which represented the gelation time (60 min). After 90 min, $G' > G''$, it showed a progressive shift from solution-like behavior to solidlike behavior, suggesting the formation of a elastically like cross-linked polymer network.

dx.doi.org/10.1021/jp303710d | J. Phys. Chem. B 2012, 116, 12038−12047

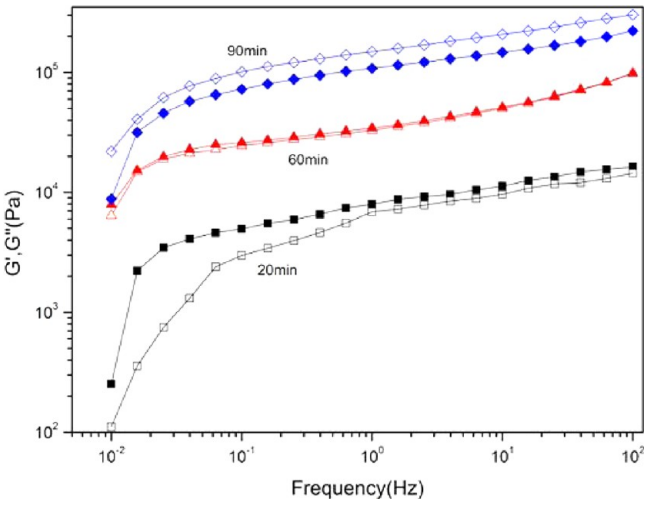

Figure 7. Evolution of elastic modulus, G' (open symbols), and viscous modulus, G'' (full symbols), as a function of frequency, during the formation of a physical hydrogel (PAA-*g*-mPEG 750-a).

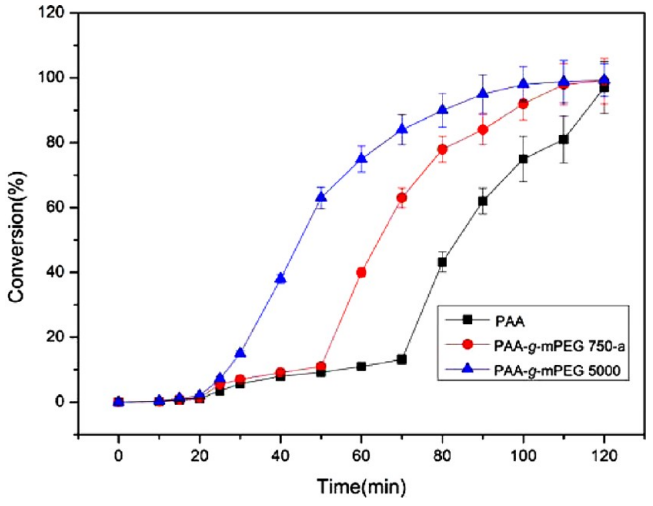

Figure 8. Monomer conversion as a function of time for physical hydrogel polymerization at the polymer concentration of 0.05 mol/L. (average value ± SD, n = 3).

We systematically observed the PAA-*g*-mPEG hydrogels gelation time (Table 3), and it was noted that PAA-*g*-mPEG

Table 3. Gelation Time for Hydrogels with Different Chain Architecture

sample	PAA	PAA-*g*-mPEG750-a	PAA-*g*-mPEG 2000	PAA-*g*-mPEG 5000
gel time/min	85	60	54	42

5000 showed the shortest gelation time around 42 min followed by PAA-*g*-mPEG 2000 (54 min), PAA-*g*-mPEG 750-a (60 min), and linear PAA (85 min). These results demonstrated that the gelation time was inversely proportional to branch chain length, where the sample containing the longest side chain of mPEG showed the shortest gelation time and could easily form networks. That is, for the hydrogel with longer branch chains, it would be easier for chains to entangle and form integral network structure, so less time was needed before gel point onset, which can be considered that the introduction of branch chain contributed to the hydrogel network formation. In addition, combined with monomer conversion profile in Figure 8, it showed that the monomer conversion rate of PAA-*g*-mPEG with branch architecture was faster than that of the linear PAA one, which further confirmed that the branch architecture facilitated the gelation process.

It is well-known that the formation of entanglement is intimately related to (1) polymer molecular weight M, specifically, it is accepted that the entanglement phenomenon is observed if M is above a critical value, which is defined as M_{crit}; and (2) initial concentration of polymer, $C > C_{crit}$, corresponding to the critical polymer concentration for gelation onset.[19,20] The above requirements need to be satisfied before polymer chain entanglement phenomenon occurs: at a minimum condition for a polymerization system, the molecular weight of polymer chain ($M > M_{crit}$) at some polymer concentration ($C > C_{crit}$) to offset of solvent dilute out entanglement junctions. Consideration value of M is easily accessible, which provides the window to define the level of entanglement and critically examine the relationship between the gel point and M. Herein, we observed polymer concentration over a wide range of 0.002−0.1 mol/L, and measured the polymer chain critical molecular weight at the gelation effect onset. For each polymer concentration, an approximate critical molecular weight range was present, and the result indicated that a high value of C always corresponded to a low value of M_{crit} (Figure 9). The most important reason

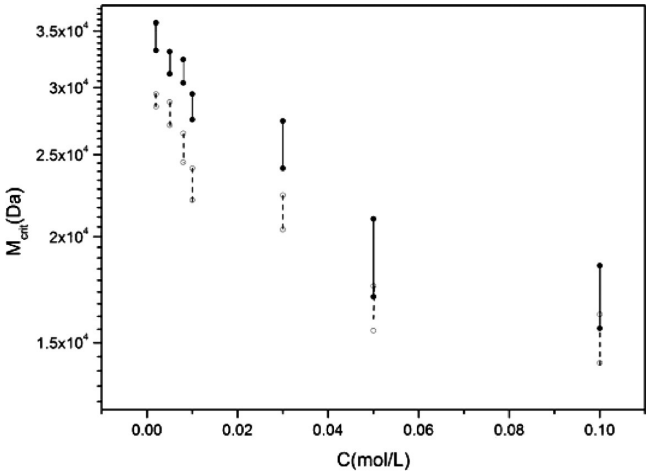

Figure 9. Estimation for the critical molecular weight at the onset of gelation as a function of polymer concentration (PAA for full symbols and PAA-*g*-mPEG 750-a for open symbols).

for this trend probably corresponded to an increase of involvement of polymer chains by forming hydrogen bonds. The second reason was related to an increase of the viscosity of the medium, which is in agreement with an increase of the density of chain entanglement. Besides, it was found that the presence of mPEG as PAA backbone branch chain would lead to a decrease in the value of M_{crit}. For example, the value of M_{crit} = 17 000 Da was observed for linear PAA gelation onset, whereas that value decreased to 15 500 Da for the sample with branch architecture to observe the gelation (at the concentration of 0.05 mol/L), indicating that the incorporation of branch length contributed to the polymer chain entanglement compared with that of linear PAA chains at a given polymer initial concentration.

dx.doi.org/10.1021/jp303710d | J. Phys. Chem. B 2012, 116, 12038−12047

Below C_{crit} and M_{crit}, we are in a situation where there may exist nanoaggregated polymer chain precursors, but they are still at a relatively isotropic state from a homogeneous solvent phase. At or above C_{crit} and M_{crit}, there appears critical phenomenon corresponding to phase separation between a homogeneous phase containing isolated chains in the solvent (sol phase) and the inorganic/organic nanoparticles constituted of aggregates of polymer chains entrapped phase (gel phase). Thus, the sol−gel transition is drastically in favor of polymer chain entanglement when $C > C_{crit}$ and $M > M_{crit}$. This trend should be a progressive condensation of entangled chains, up to when a full macroscopic entanglement from the origin of phase separation is attained. This mechanism can be illustrated by a scheme presented in Figure 10 after taking into account the above two key aspects. Haraguchi et al. also noted that the nanocomposite gels cannot form uniform networks or showed brittle property when the polymer concentration was below a certain value, while a significant increase of strength and modulus was observed above this concentration.[11] It is clear that only a condition of polymer concentration approaching the critical value is satisfied before the progressive formation of a real cross-linked network onset and construction of a homogeneous macroscopic network.

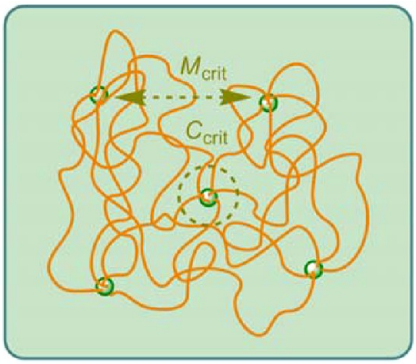

Figure 10. Schematic illustration of the two requirements before the physical cross-linked network structures formed. The length of grafted chains reaches more than a half of the distance between two neighboring SNs (M_{crit}) and the concentration of SN/polymer (C_{crit}) exceeds the critical concentration. The dynamic percolation-to-cluster transition occurs and the cross-linked network is formed.

3.3. Hydrogels Swelling Behavior. The dry hydrogels were immersed in water and their swelling behaviors as a function of time are illustrated in Figure 11. One can note that the hydrogels (PAA, PAA-*g*-mPEG750-a) swelled significantly at the early stage until swelling ratios attained the transient maximal values around 26 h, then they reached the final equilibrium values of 300−500. Here, the hydrogels in this study were applied to swelling measurement without postpurification (e.g., dialysis against water) after preparation; thus, this characteristic swelling−deswelling behavior was ascribed to the polymer chains that did not actually graft onto the SNs and dissolved out of the network structure.[26] It should be mentioned that this unique phenomenon is different from the thermosensitive polymers (e.g., *N*-isopropylacrylamide, PNIPA) that transfer from coil-to-globule at the lower critical solution temperature (LCST).[29] For the hydrogel of PAA-*g*-mPEG2000 it showed much normal swelling behavior without obvious dissolution phenomenon although its equilibrium swelling ratio was much lower than that of PAA. This

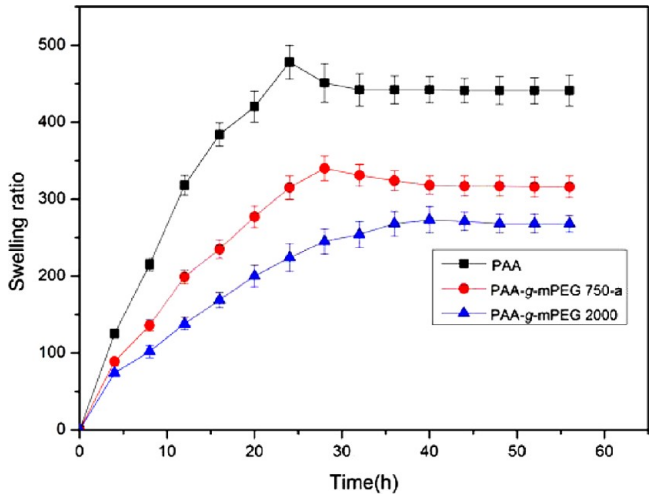

Figure 11. Swelling behaviors for hydrogels with different architectures at 25 °C.

result is reasonable if we consider the fact that the introduction of mPEG not only decreases the polymer hydrophilicity but also increases the chain entanglements that reinforce the network rigidity, and bring more resistance against water molecules penetreating into the networks. After another careful observation in Figure 11, one can further note that the time to attain swelling equilibrium increased with increasing of branch length, which can be explained that the long branch structure contributed to the compacted network structure and an increase in cross-linking density (ν) at a given SN concentration.

3.4. Branch Architecture on Gel-to-Sol Transition. The dissolution of a polymer into a solvent involves two transport processes, namely solvent diffusion and polymer chain disentanglement.[30] The polymer interaction entanglement is entropically less favorable and is promoted by noncovalent weak force. Thus, the polymer chains' entanglements can be disturbed by external stimuli; e.g., temperature perturbation and mechanical agitation can accelerate the dissolution process.[26] Here, we monitored the gel-to-sol transition process, including swelling ratio, mass loss, and gel-to-sol transition temperature ($T_{g\text{-}s}$), in heated water and found that (1) the presence of nonpermanent polymer chains' physical entanglements within cross-linked network structure can be eventually disturbed by outside energy and cause bulk dissolution (flowable sols fraction), and (2) the thermally triggered gel-to-sol transition of PAA was greatly hindered by the interactions between SN and polymer chains, where polymer branch architecture dominated the specific hydrogel dissolution process (Figure 12).

It is well-known that the dissolution process is disassociation-controlled if the polymer diffusion rate in a liquid layer adjacent to the polymer−solvent interface is faster than the dissociation rate, or diffusion-controlled if the diffusion rate is slower than the dissociation rate.[30] Considering that the PAA-*g*-mPEG-based hydrogels possessed a high swelling ratio, the dissolution process can be regarded as a disassociation-controlled one (the solvent flux into the polymer is sufficient to carry away all the chains that dissolved from the gel into the liquid). Herein, the sample of PAA-*g*-mPEG 2000 was chosen to observe the whole swelling-dissolution process in excessive water at 62 °C without agitation (Figure 12a). One can note that, at initial swelling stage, the hydrogel hydrophilicity dominated the trend, the

dx.doi.org/10.1021/jp303710d | J. Phys. Chem. B 2012, 116, 12038−12047

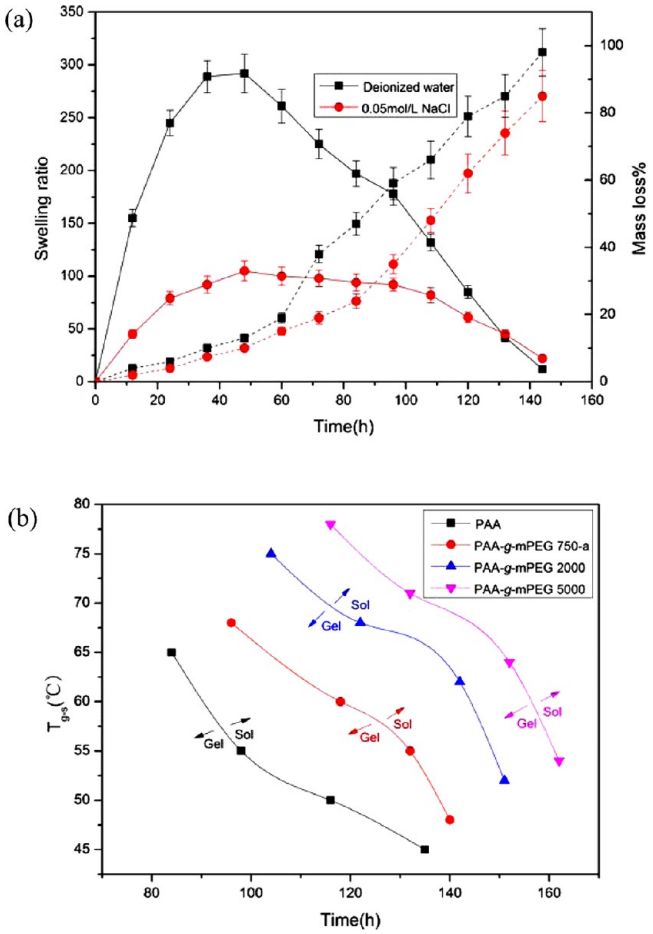

Figure 12. Physical hydrogel dissolution process: (a) PAA-*g*-mPEG 2000 swelling ratio and mass loss ratio as function of time at 62 °C (solid lines refer to swelling ratio, and dash lines refer to mass loss), and (b) the gel−sol phase transition of hydrogels with different branch lengths.

swelling ratio increased with time, and the mass loss ratio was still low at this period. Subsequently, the bulk of hydrogel started the dissolution process where mass loss increased rapidly. This result indicated that the polymer chains disentangled and the cross-linked network structure was under disturbance, and this stage continued until the hydrogel dissolution process completed. Another careful observation in Figure 12a, one can note that the dissolution process decreased with an increase of solution ionic strength (0.05 mol/L NaCl). This behavior is justified if we consider that the PAA belongs to ionic-type polymer and it is easily subjected to ionic charge shielding influence, which causes the chains to present a coil conformation, and thus there is more resistance against disentanglement and the dissolution process is limited thereafter, while for the gel-to-sol transition process, the values of $T_{g\text{-}s}$ increased significantly as the polymer branch length increased (Figure 12b). This result further reveals that the degree of polymer entanglement increases due to more chains involving in the intramolecular action; that is, there is higher friction for chains to disentangle and thus contributes to the network rigidity.

Recognizing the presence of entanglements in polymers, the gel-to-sol transition could be understood as a process undergone by the polymer chains from original entangled gel-like phase to a disentangled sol phase.[31,32] Thus, the dimensional change of nanoaggregated microgel for physical hydrogels dissolution was monitored at interval times via DLS measurements at a very low concentration ($\sim 10^{-4}$ g/L). The divergent hydrodynamic radii of SNs, *r*, suggesting topological difference between linear PAA and bottle-brush-like PAA-*g*-mPEG chains conformations, are exhibited in Figure 13. Here,

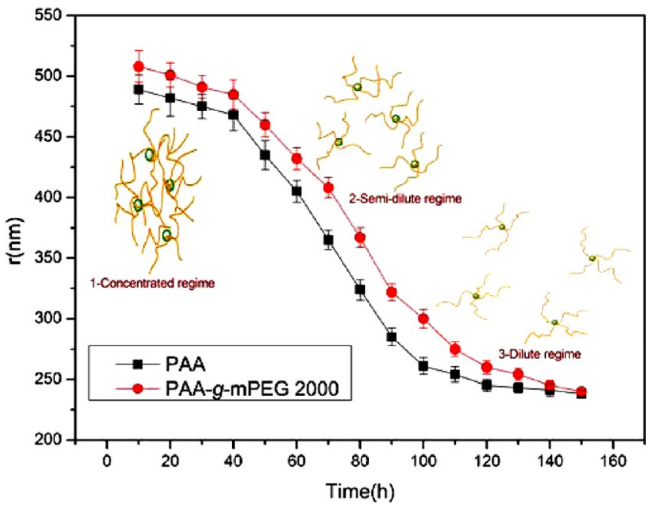

Figure 13. Dissolution of physical hydrogels resulting in changes of inorganic/organic nanoparticles hydrodynamic radii. The inset schemes illustrate polymer dissolution and chains disentanglement process: (1) initial polymer chains present coil conformation with no disentanglement, which corresponds to a swellable system; (2) beginning of the disentanglement stage showing the decrease dimension of coil conformation polymer size, which depicts the onset of dissolution in the diffusion boundary layer; and (3) continuation of disentanglement leading to the complete dissolution and the disentangled chains exhibit free Brownian motion in the solvent.

the radii of SNs coated by PAA-*g*-mPEG were significantly larger than those coated by linear PAA ones, indicating a higher degree of entanglement over the network structure and a slower dissolution process. Besides, this architectural difference between two polymer chains resulted in distinct dissolution profiles and the dimensional stability was enhanced by the addition of branch architecture. After another careful observation, one can note that the whole profile could be divided into three typical stages: initially, the polymer chains entangled closely among each other and led to a high value of *r*, then a sharp decay in the measured *r* value was subsequently observed at the continued dissolution stage, and it gradually reached the equilibrium after ∼120 h under the given experimental conditions. As the hydrogel network continued to collapse, the bulk gel eventually dissolved into a collection of oligomer inorganic/organic nanoparticles under more free-moving status. Therefore, the kinetics of hydrogel network dissolution provides more insight into the cross-linked network structure: (1) the SNs in situ initiated hydrogels illustrate a three-stage decrease in *r* within dissolution process, and this decay is a characteristic of bulk polymer chains' disentanglement process, where the dissolution rate generally decreases as polymer chains depleting from cross-linked network structure; (2) the PAA-*g*-mPEG chains tend to be more efficiently incorporated into entanglement during the gelation process comparing with the linear PAA chains, and they contribute a more stable cross-linked network structure.

dx.doi.org/10.1021/jp303710d | *J. Phys. Chem. B* 2012, 116, 12038−12047

3.5. Branch Architecture on Mechanical Strength. The mechanical properties of hydrogels including tensile strength and elasticity are indispensable factors in their practical applications.[6−12] Therefore, the hydrogels with different branch lengths were applied to mechanical property measurements, and their stress−strain profiles are shown in Figure 14. It can be

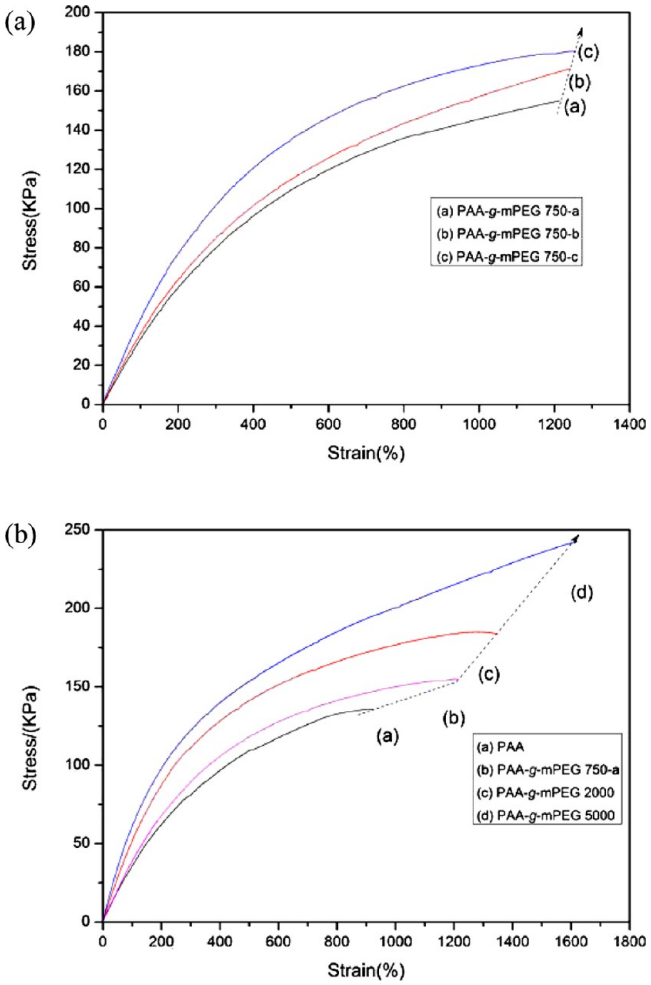

Figure 14. Stress−strain curves of hydrogels with different branch structures: (a) hydrogels with different branch fractions, and (b) hydrogels with different branch lengths.

found that the both tensile stress and elongation at break increased with branch fraction as well as branch length, indicating the incorporation of branch chains contributed to close entanglements and ability of the physical cross-links to dissipate energy during deformation. Here we interpreted the force−extension data by the Flory simple statistical theory (SST)[19,20] to estimate the molecular weight of two consecutive entanglements, M_e. The network chain density, N, is related to the shear modulus, G, via following equation

$$G = NkT \tag{1}$$

where k is the Boltzmann constant and T the absolute temperature. In a tensile-extension experiment, G is approximated to $\sigma/(\lambda - \lambda^{-2})$, where σ is the force per unit unstrained area and λ the extension ratio. In terms of M_e, one has

$$\sigma/(\lambda - \lambda^{-2}) = (\rho RT{v_2}^{2/3}/M_e)(1 - 2M_e/M) \tag{2}$$

where is ρ the density, R the gas constant, and v_2 the volume fraction of polymer in swollen gel. The initial slope of the σ versus $\lambda - \lambda^{-2}$ plot is equated to the right-hand side of eq 2 and the value of molecular weight between two neighboring cross-links (entanglements) can be calculated (Table 4). It is noted

Table 4. Calculation of M_e Values from Eq 2

sample	PAA	PAA-*g*-mPEG 750-a	PAA-*g*-mPEG 750-b	PAA-*g*-mPEG 750-c	PAA-*g*-mPEG 2000	PAA-*g*-mPEG 5000
M_e[a]	2045	1763	1751	1455	1307	1210

[a]Assuming $v_2 = 0.167$, $\rho = 1.22$ g/cm^3,[33] $T = 298$ K for all the samples.

that the value of M_e decreased with increasing branch length and the degrees of entanglement dominated the gel strength, suggesting M_e depended upon the length as well as number of branch chains.

Here, we studied the branch structure by tailoring the molar ratio and length of mPEG with backbone and discussed it in relation to the network mechanical properties. For example, the PAA linear chains entanglements were sufficient to provide hydrogels as high as 136 KPa stress, while the incorporation of branch structure further facilitated the formation of entangled network and more amount of cross-link junctions firmly entrenched within the networks. That is, with increasing branch fraction from 1 to 5 mol % at a fixed length, the tensile strength increased from 154.9 to 180.4 KPa with a most constant elongation at break (Figure 13a). Meanwhile, with increasing length of the branch structure from 750 to 5000 Da at a fixed molar fraction, the both tensile strength and elongation at break increased almost proportionally to the length, which contributed to the greater elastic strength by means of participation in physical entanglements (Figure 13b). Therefore, the mechanical properties of hydrogels were directly related to their chains' entanglement, where each chain in the system was constrained by several junctions and the network became more rigid and could endure a high level of deformation.[19]

As shown by the dashed line in Figure 13a,b, the tensile strength increased at first with increasing molar fraction of branch structure, while the elongation remained almost constant (the number of the chain end per unit molecular weight changed with the branch length, but it kept constant against the change in the number of branches, due to the branch length being uniform and predetermined by the molecular weight of the original macromonomer), and then in the next stage, the both tensile strength and elongation at break increased with further increase in length of branch. This mechanical characteristic change in stress curves with branch structure may suggest the following mechanism for influences of branch conformation on network strength. That is, in the first stage, where the tensile strength increases, it corresponds to the increase in the number of cross-links (physical entanglements) with increasing fraction of branch structure and the three-dimensional network throughout the hydrogel has not fully formed yet; thus, the primary cross-linked architecture at this stage is further developed on the basis of original linear PAA network structure. Then, the subsequent stage, where both tensile strength and elongation at break increase, corresponds to the further mature network structure formation process and more amount of entanglement, i.e., increase of network density and volume to produce polymer chain closer entanglements.

dx.doi.org/10.1021/jp303710d | J. Phys. Chem. B 2012, 116, 12038−12047

4. CONCLUSIONS

The study here presents new aspects of the formation of tough and flexible hydrogels with a copolymer of PAA as backbones and mPEG acrylate as branch chains in aqueous solutions, in the absence of organic cross-links, thanks to the close entanglements among polymer chains with various architectures. A series of hydrogels with different branch architectures were synthesized to study the effect of branch chain on hydrogels properties, and the results indicated that the bottlebrush-like branch architecture significantly affected the swelling behavior, gel-to-sol transition, and mechanical properties. The introduction of multibranch chains to linear chains could further reinforce the intermolecular chain entanglement couplings for the poly(macromonomer)s structure and contributed to the network rigidity and rubber-like elasticity behavior. The hydrogels gel-to-sol transition temperature and measurements of molecular weight between two consecutive entanglements indicated that the branch chains reinforced the level of entanglement and enhanced the network stability. This analysis of chain entanglements by different polymer chain architectures extends the understanding of the formation physical hydrogels from the inorganic/organic nanoparticles interactions, and makes future fabrication of high mechanical strength hydrogels more controllable and accessible.

AUTHOR INFORMATION

Corresponding Author

*Tel.: 86-10-62773607. Fax: 86-10-62784550. E-mail: xxmdce@mail.tsinghua.edu.cn.

Notes

The authors declare no competing financial interest.

ACKNOWLEDGMENTS

We are grateful for funding from the National Natural Science Foundation of China (51073088, 91023027, 50573038, and 20874056).

REFERENCES

(1) Vermonden, T.; Censi, R.; Hennink, W. E. *Chem. Rev.* **2012**, *112*, 2853−2888.
(2) Samchenko, Y.; Ulberg, Z.; Korotych, O. *Adv. Colloid Interface Sci.* **2011**, *168*, 247−262.
(3) Malmsten, M. *Soft Matter* **2011**, *7*, 8725−8736.
(4) Jennifer, N C; Brent, S. S. *Polymer* **2011**, *52*, 4631−4643.
(5) Jinah, K.; Cheng, C. P.; Anuj, C. *J. Controlled Release* **2010**, *148*, 110−116.
(6) Li, Z. Q.; Wang, F.; Guan, J. J. *Biomacromolecules* **2009**, *10*, 3306−3316.
(7) Zhao, S. P.; Zhang, L. M.; Ma, D.; Yang, C.; Yan, L. *J. Phys. Chem. B* **2006**, *110*, 16503−16507.
(8) Gong, J. P. *Soft Matter* **2010**, *6*, 2583−2590.
(9) Okumura, Y.; Ito, K. *Adv. Mater.* **2001**, *13*, 485−487.
(10) Haraguchi, K.; Ebato, M.; Ohbayashi, A.; Takehisa, T. *Adv. Mater.* **2006**, *18*, 2250−2254.
(11) Haraguchi, K.; Farnworth, R.; Ohbayashi, A.; Takehisa, T. *Macromolecules* **2003**, *36*, 5732−5741.
(12) Huang, T.; Xu, H. G.; Wang, H. L. *Adv. Mater.* **2007**, *19*, 1622−1626.
(13) Na, B.; Lv, R. H.; Xu, W. F.; Yu, P. S.; Wang, K.; Fu, Q. *J. Phys. Chem. B* **2007**, *111*, 13206−13210.
(14) Read, D. J.; Jagannathan, K.; Likhtman, A. E. *Macromolecules* **2008**, *41*, 6843−6853.
(15) Flory, P. J.; Rehner, J. *J. Chem. Phys.* **1943**, *1*, 512−520.
(16) O'Neil, G. A.; Wisnudel, M. B.; Torkelson, J. M. *Macromolecules* **1996**, *29*, 7477−7490.
(17) Graessley, W. W. *Polymer* **1980**, *21*, 258−262.
(18) Kunamaneni, S.; Buzza, D. A.; Read, D. J.; Larsen, A. L. *Macromolecules* **2006**, *39*, 6720−36.
(19) Flory, P. *J. Chem. Rev.* **1944**, *35*, 51−57.
(20) Flory, P. J. *Ind. Eng. Chem.* **1946**, *38*, 417−436.
(21) Moeinzadeh, S.; Khorasani, S. N.; Ma, J. Y.; He, X. Z.; Jabbari, E. *Polymer* **2011**, *52*, 3887−3896.
(22) Dorset, D. L.; Baugh, L. S.; Luo, J.; Shea, K. J. *J. Phys. Chem. B* **2011**, *115*, 8858−8863.
(23) Lee, J. H.; Driva, P.; Hadjichristidis, N. *Macromolecules* **2009**, *42*, 1392−1399.
(24) Zou, H.; Wu, S. S.; Shen, J. *Chem. Rev.* **2008**, *108*, 3893−3957.
(25) Banet, P.; Griesmar, P; Serfaty, S.; Vidal, F.; Huerou, V. J.; Le., J. Y. *J. Phys. Chem. B* **2009**, *113*, 14914−14919.
(26) Yang, J.; Wang, X. P.; Xie, X. M. *Soft Matter* **2012**, *8*, 1058−1063.
(27) Yang, J.; Shi, F. K.; Cheng, G.; Xie, X. M. *J. Colloid Interface Sci.* **2012**, *381*, 107−115.
(28) Stöber, W.; Fink, A.; Bohn, E. *J. Colloid Interface Sci.* **1968**, *26*, 62−69.
(29) Ren, H. Y.; Zhu, M. F.; Haraguchi, K. *Macromolecules* **2011**, *44*, 8516−8526.
(30) Vrentas, J. S.; Vrentas, C. M. *J. Polym. Sci. B Polym. Phys.* **1998**, *36*, 2607−2614.
(31) Miller-Chou, B. A.; Koenig, J. L. *Prog. Polym. Sci.* **2003**, *28*, 1223−1270.
(32) Narasimhan, B.; Peppas, N. A. *J. Polym. Sci. B Polym. Phys.* **1996**, *34*, 947−961.
(33) Mark, J. E. *Polymer Data Handbook*; Oxford University Press: Oxford, UK, 1999; p 252.